LANGMUIR

pubs.acs.org/Langmuir Article

Rapid Precipitation of Ionomers for Stabilization of Polymeric Colloids

Douglas M. Scott,[‖] Arash Nikoubashman,*[,‖] Richard A. Register, Rodney D. Priestley, and Robert K. Prud'homme*

Cite This: *Langmuir* 2023, 39, 570−578 Read Online

ACCESS | Metrics & More | Article Recommendations | Supporting Information

ABSTRACT: Polymeric colloids have shown potential as "building blocks" in applications ranging from formulations of Pickering emulsions and drug delivery systems to advanced materials, including colloidal crystals and composites. However, for applications requiring tunable properties of charged colloids, obstacles in fabrication can arise through limitations in process scalability and chemical versatility. In this work, the capabilities of flash nanoprecipitation (FNP), a scalable nanoparticle (NP) fabrication technology, are expanded to produce charged polystyrene colloids using sulfonated polystyrene ionomers as a new class of NP stabilizers. Through experimental exploration of formulation parameters, increases in the ionomer content are shown to reduce the particle size, mitigating a significant trade-off between the final particle size and inlet concentration; thus, expanding the processable material throughput of FNP. Further, the degree of sulfonation is found to impact stabilization with optimal performance achieved by selecting ionomers with intermediate (2.45−5.2 mol %) sulfonation. Simulations of single ionomer chains and their arrangement in multicomponent NPs provide molecular insights into the assembly and structure of NPs wherein the partitioning of ionomers to the particle surface depends on the polymer molecular weight and degree of sulfonation. By combining the insights from simulations with diffusion-limited growth kinetics and parametric fits to experimental data, a simple design formulation relation is proposed and validated. This work highlights the potential of ionomer-based stabilizers for controllably producing charged NP dispersions in a scalable manner.

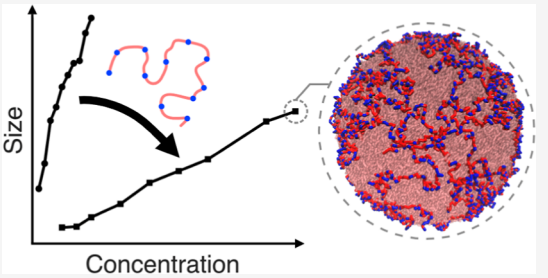

INTRODUCTION

Polymer nanoparticles (NPs) have shown immense promise and demonstrated effectiveness for use in a wide range of applications, such as encapsulation of active pharmaceutical ingredients,[1,2] supports for catalysts,[3] Pickering emulsifiers,[4,5] and colloidal crystal formers.[6] The broad applicability of these polymer-based NPs can be attributed to the diversity of available monomer chemistries and rich phase behavior of polymers, enabling the formation of complex morphologies including the core−shell, Janus, and multifaceted geometries.[7,8] Polymeric NPs can be produced using various techniques, including emulsion polymerization of monomers, or precipitation-mediated approaches involving the solvent stripping of emulsions or microfluidic-templated solvent exchange of solutions containing preformed polymers.[9−11] However, approaches for the synthesis of more complex NP structures can face limitations involving scalability and chemical versatility. To overcome these challenges, flash nanoprecipitation (FNP) has proven to be a versatile and scalable process for forming not only polymeric colloids with various compositions and morphologies[3,7,12] but also as a process for encapsulating active pharmaceutical ingredients and vaccines.[13−16]

In FNP, polymeric NPs are fabricated through the supersaturation and precipitation of polymers, driven by the rapid mixing of a polymer solution with a miscible antisolvent.[17,18] The resulting aggregates need to be stabilized through the creation of steric or electrostatic barriers to prevent macroscopic precipitation. To this end, amphiphilic block copolymers (BCPs) are commonly added to the formulation, which adsorb onto the surface of growing aggregates to form sterically repulsive brush layers.[19−22] Additionally, for the FNP of purely hydrophobic polymers (e.g., polystyrene, polyisoprene, and so forth) with water as the antisolvent, the adsorption of naturally present anions (HCO_3^-, OH^-) has been shown to induce a negative surface potential (∼−30 mV) on aggregates which are, therefore, electrostatically stabilized.[23,24]

Since the relative time scales of stabilization and polymer aggregation dictate the final particle size, formulation

Received: October 18, 2022
Revised: December 13, 2022
Published: December 28, 2022

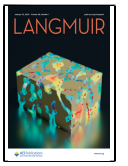

https://doi.org/10.1021/acs.langmuir.2c02850
Langmuir 2023, 39, 570−578

parameters, such as the stabilizer concentration (in the case of BCPs) and core material concentration, can be adjusted to achieve desired particle sizes.[20] For example, as the core concentration increases, the initial number density of collapsed polymer nuclei also increases, thereby reducing diffusion length scales and accelerating aggregation to yield larger NPs.[25]

Applications involving Pickering emulsifiers or colloidal crystals require formulations with controlled NP size, surface potential, and hydrophobicity—a combination of properties that has not been previously studied for FNP. However, current stabilization methods for FNP present challenges for controlling these properties: (1) adsorbed BCP monolayers on NP surfaces have been shown to denature at water/hydrophobic interfaces, compromising the structure and long-term stability of interfacially adsorbed NPs[26] and (2) adsorption of anions strongly depends on the chemistry of the constituent polymers and the surrounding liquid phase. Thus, production of NPs with moderately hydrophobic surfaces, such as those that are required for Pickering emulsifiers, presents a processing challenge for FNP; operating at high-solid loading can lead to NP aggregation, whereas processing at low concentrations results in dilute NP dispersions, requiring subsequent concentrating steps to achieve desired concentrations for applications.[27−29]

These challenges could be overcome by controllably introducing electrostatic-mediated stabilization of NPs while retaining adequate surface hydrophobicity. To this end, a promising strategy amenable to FNP is the introduction of ionomers, that is, hydrophobic polymers with a small portion of monomers containing ionizable functional groups (typically <15 mol %). Previous experiments using pure solutions of ionomers have demonstrated the formation of NPs from the collapse and aggregation of chains as the solvent quality worsened during mixing with subsequent stabilization through the outward expression of charged monomers.[30−32] By blending ionomers with lower-cost neutral polymers to form the majority of the NP core volume, charged NPs with similar sizes and properties may be produced at an overall lower cost while allowing a selection of diverse polymer chemistries for the cores, independent of the ionomer chemistry.

In this work, we apply this approach to mixtures of neutral and charged polymers for the scalable production of charged NP dispersions. We investigate experimentally the impact of formulation parameters on final NP properties, accompanied by molecular simulations to elucidate the internal structure of the formed NPs. The key structural question is whether the ionic monomers are uniformly distributed throughout the NP, which would be entropically favored, or localized on the NP surface, which would be favored by the partition coefficient of the ionic monomers into the aqueous phase. Finally, a discussion of the underlying mechanisms for stabilization leads to a simple design equation for NP formulation.

METHODS AND MATERIALS

Materials. Polystyrene (PS; M_w = 35 kg/mol, $Đ$ = 2.2)[33] was purchased from Sigma-Aldrich (St. Louis, Missouri). Poly(styrene-*r*-sodium styrene sulfonate) (abbreviated "iPSS") samples of varying degrees of sulfonation (f_{sulf} = 1.48, 2.45, 5.2, and 9.7 mol %), synthesized from a PS precursor (M_w = 299 kg/mol, $Đ$ = 2.4; Dow Chemical Co., Midland, Michigan) and characterized in a prior study,[34] were provided for the current work. Tetrahydrofuran (THF, HPLC grade) was purchased from Fisher Scientific. Purified deionized (DI) water was obtained from a Milli-Q IQ 7000 ultrapure system.

NP Fabrication and Characterization. To produce NPs, 0.5 mL of an organic feed solution containing PS and iPSS in THF was manually injected into one inlet of a confined impingement jet (CIJ) mixer at the same time as 0.5 mL of DI water was injected into the second inlet (antisolvent stream). The total flow rate into the mixer was approximately 2 mL/s. The effluent of the mixer was directed into a stirred 4 mL reservoir of DI water for a final cumulative 10-fold dilution, resulting in a final solvent composition of 10% THF and 90% H_2O.

Particle size was measured by dynamic light scattering (DLS) on an Anton Paar Litesizer 500 (Anton Paar, Graz, Austria) with a 658 nm laser and side scatter detection angle of 90°. In particle-size measurements, NP dispersions were diluted to 0.1 mg/mL in DI water before measurement in polystyrene cuvettes (path length = 10 mm). Particle diameters reported are the harmonic intensity (*Z*-)averages. The polydispersity index (PDI) is obtained from the Taylor series expansion of the autocorrelation function and is implemented into the Anton Paar Kalliope data analysis software. A ratio of the second to the first moment is defined as the PDI, where values of 0.1 are generally obtained for monodisperse particles.[35,36]

Molecular Dynamics Simulations. Polymers are modeled as bead-spring chains,[5,7,8,24] consisting of spherical beads of diameter σ and mass m. Each bead represents roughly one Kuhn segment, where we have assumed that the sulfonated groups in the iPSS chains have the same statistical segment length as PS. In this model, each PS and iPSS chain consists of N_{PS} = 49 and N_{iPSS} = 417 beads, respectively, and the positions of the $f_{sulf} \times N_{iPSS}$ sulfonated groups (SS beads) are drawn randomly for each iPSS chain (unless stated otherwise explicitly). This mapping leads to $\sigma \approx 1.5$ nm,[24] which is used to convert the length scales in our simulations to experimental units. Bonded interactions are modeled *via* the finitely extensible nonlinear elastic (FENE) potential[37]

$$U_{FENE}(r) = \begin{cases} -\frac{1}{2}kr_0^2 \ln[1-(r/r_0)^2], & r < r_0 \\ \infty, & r \geq r_0 \end{cases} \quad (1)$$

with spring constant $k = 30k_BT/\sigma^2$ and maximum extension $r_0 = 1.5\sigma$ to prevent unphysical bond crossing.[38]

We neglect an explicit treatment of long-range electrostatic charge effects in our simulations due to the modeling complexities arising from the inherent heterogeneity of the dielectric constants in our systems[39,40] and from the potential adsorption of dissolved ions on the NP surface,[23] which cannot be resolved at the employed level of coarse graining.[41] Instead, we implicitly include charge effects into our model by treating the SS repeat units as hydrophilic entities on a hydrophobic chain. Nonbonded interactions between beads of the same type (S−S and SS−SS pairs) are given by the Lennard−Jones (LJ) pair potential

$$U_{LJ}(r) = \begin{cases} 4\varepsilon\left[\left(\frac{\sigma}{r}\right)^{12} - \left(\frac{\sigma}{r}\right)^{6}\right], & r \leq r_{cut} \\ 0, & r > r_{cut} \end{cases} \quad (2)$$

with interaction strength $\varepsilon = k_BT$ and cutoff radius $r_{cut} = 3\sigma$. In contrast, S−SS pairs interact *via* the purely repulsive Weeks−Chandler−Andersen (WCA) potential,[42] which is obtained by truncating eq 2 at $r = 2^{1/6}\sigma$ and shifting it by ε. The surrounding solvent is modeled explicitly as a liquid of LJ particles, with the same size and mass as the polymer beads, at a number density of $\rho_{slv} = 0.66\sigma^{-3}$. At this level of coarse graining, each liquid bead represents multiple water and THF molecules, which can be considered as homogeneously mixed at the spatial resolution of our simulation model.[43] In this simplified representation, we can mimic the solvent exchange by gradually changing the pair interaction between the polymer beads and solvent particles in the system[24,44]

$$U_{slv}(r) = \lambda U_{WCA}(r) + (1-\lambda)U_{LJ}(r) \quad (3)$$

https://doi.org/10.1021/acs.langmuir.2c02850
Langmuir 2023, 39, 570−578

The dimensionless parameter $0 \leq \lambda \leq 1$ controls the solvent quality, with good solvent conditions for $\lambda = 0$, θ-conditions for $\lambda \approx 0.05$, and poor solvent conditions for $\lambda \gtrsim 0.5$. When the chains are dispersed in pure THF, we set $\lambda_{S\text{-}slv} = 0$ for the S-solvent interactions and $\lambda_{SS\text{-}slv} = 0.5$ for the SS-solvent interactions. As water is added, $\lambda_{S\text{-}slv}$ is gradually increased to 0.5, while $\lambda_{SS\text{-}slv}$ is gradually reduced to 0.

Single-chain simulations have been carried out in cubic boxes with edge length $L_{box} = 80\sigma$ and periodic boundary conditions applied to all directions. The multi-chain simulations for studying NP formation have been conducted in a cubic box with $L_{box} = 100\sigma$ at a monomer number density of $\rho_m \approx 0.16\sigma^{-3}$. In those simulations, we have included semi-permeable walls at the edges of the simulation box which repel the polymer beads but let the solvent particles through, to impede the formation of system-spanning structures. For these parameters, the resulting spherical NPs have a diameter of about 110 nm. All simulations have been conducted in the canonical ensemble, where the temperature was controlled using a Nosé−Hoover thermostat. The equations of motion were integrated using a velocity Verlet algorithm with timestep $\Delta t = 0.005\tau_{MD}$, with time scale $\tau_{MD} = 0.28$ ns, as established in our previous work.[24] All simulations have been performed using the HOOMD-blue simulation package (v. 2.9.7).[45]

RESULTS AND DISCUSSION

We used FNP to incorporate ionomer stabilization, as shown in Figure 1. In brief, solutions of PS (M_w = 35 kDa) and iPSS

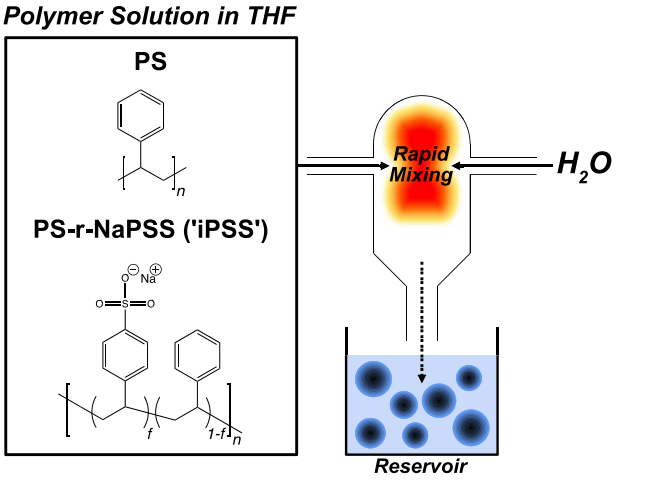

Figure 1. Schematic of the FNP process and description of the formulation parameters for iPSS-induced stabilization.

(M_w = 299 kDa for PS precursor) in THF were rapidly mixed with an equal volume of water in a CIJ mixer to effect precipitation before further dilution into a water reservoir. An understanding of ionomer-driven stabilization and formulation heuristics was achieved by adjusting parameters including the total inlet mass concentration (c), the weight percent of iPSS (w_{iPSS}) in the inlet stream, and the degree of sulfonation of the iPSS chains used (f_{sulf}).

We measured the size of the precipitated NPs *via* DLS, and the effects of polymer concentration (c) and ionomer weight fraction (w_{iPSS}) on resultant NP size for formulations with moderate sulfonation (f_{sulf} = 5.2 mol %) are shown in Figure 2a. The particle size increases with increasing c, a typical result

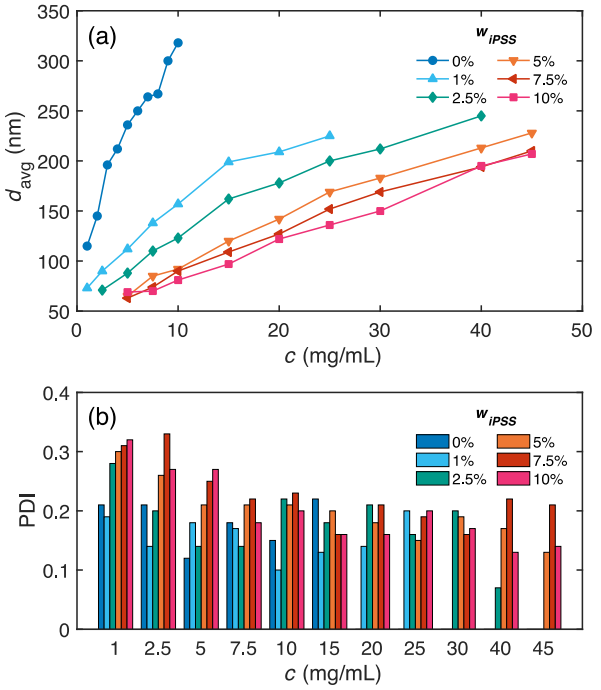

Figure 2. Effect of formulation parameters, total inlet polymer concentration (c) and ionomer weight percent (w_{iPSS}), on particle size distributions: (a) harmonic intensity-averaged diameters and (b) PDI.

for FNP, as the smaller distances between collapsed globules facilitate diffusion-limited aggregation (DLA),[46] yielding larger aggregates in shorter assembly times before the onset of stabilization. However, with increasing w_{iPSS} for fixed c, the particle size decreases, indicating that the iPSS acts as an efficient stabilizer in decreasing the number of aggregation steps before electrostatics stops further growth. For example, in 10 mg/mL of total solids, 318 nm NPs are formed at 0% iPSS, 157 nm NPs are formed in 1% iPSS, and 80−95 nm NPs are formed in 5−10% iPSS. Also note that the effect of ionomer content saturates, that is, the differences in NP sizes are less significant at higher w_{iPSS}. Additionally, for higher w_{iPSS} formulations (5−10 wt %), the processable range is extended to higher concentrations of about $c \approx 45$ mg/mL, enhancing the scalability of the FNP process. By comparison, in the case of hydrophobic anion adsorption (w_{iPSS} = 0%), the processable concentrations are limited to $c \approx 10$ mg/mL before the onset of gross aggregation and high polydispersity. For processing higher c solutions *via* FNP, the overlap concentration (c^*) represents an upper limit beyond which the precipitation of chains cannot form NPs, but rather form entangled networks.[20] In this study, PS and iPSS concentrations remain below their respective c^* (PS: $0.009 < c_{PS}/c_{PS}^* < 0.43$; iPSS: $0.0003 < c_{iPSS}/c_{iPSS}^* < 0.13$), allowing NPs to be formed for all formulations containing polymers of the given molecular weights.

While the presence of iPSS was found to reduce average NP size, the size dispersity must also be considered to evaluate the quality of produced NP dispersions. Figure 2b shows the PDI of each produced dispersion. While the NPs were found to be relatively monodispersed (PDI = 0.17 ± 0.04) at high c, the PDI was elevated for low c formulations and trended positively

https://doi.org/10.1021/acs.langmuir.2c02850
Langmuir 2023, 39, 570−578

with increasing w_{iPSS}. A representative collection of particle size distributions is presented in Figure 3a. At low concentrations, large aggregates are detected until a threshold concentration is reached beyond which unimodal particle distributions are produced. A potential explanation for this outcome is the reduction in the initial number density of PS nuclei at lower c. This, in turn, can limit the initial collision frequency between iPSS chains and growing PS aggregates, thereby introducing heterogeneity in the distribution of iPSS chains among NPs. For a portion of aggregates possessing lower iPSS content, further aggregation is allowed to proceed to yield a secondary population of large particles. Consequently, for higher w_{iPSS} formulations, c must be increased to enable the equal distribution of iPSS chains among growing aggregates. The minimum threshold concentrations for which unimodal particle distributions were produced for each w_{iPSS} tested is shown in Figure 3b. Notably, this trend couples the formulation parameters (c and w_{iPSS}) for producing unimodal particle distribution while setting the lower bound for accessible particle sizes (d_{avg} = 115 ± 14 nm).

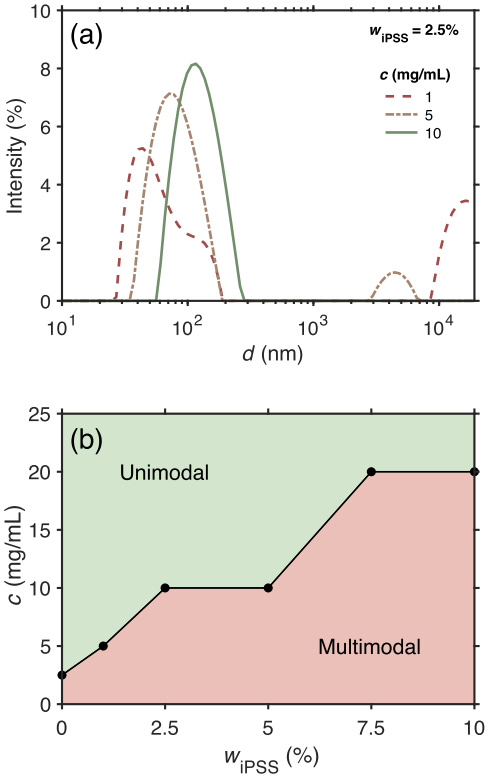

Figure 3. (a) Particle size distributions of PS and iPSS (f_{sulf} = 5.2 mol %) NPs, indicating the presence of large aggregates at lower inlet polymer concentrations (c = 1, 5 mg/mL) and unimodal distributions at higher concentrations (10 mg/mL) for w_{iPSS} = 2.5%; (b) minimum threshold concentrations for all tested w_{iPSS} above which unimodal particle size distributions are produced.

The charge content of ionomers is a key parameter dictating chain conformation, miscibility, and ultimately bulk mechanical, thermal, and transport properties due to the phase separation of charged monomers from surrounding hydrophobic monomers and solvents.[47−50] Since FNP involves a fast shift in solvent quality leading to chain collapse and monomer reorganization prior to aggregation—two events which can be impacted by the charge content of ionomers[32]—the impact of the degree of sulfonation of iPSS chains (f_{sulf}) on aggregate stabilization was also investigated. iPSS chains with increasing f_{sulf} (1.48, 5.2, 9.7 mol %) were used to produce NPs within the upper range of c (20−40 mg/mL) to reduce as much as possible polydispersity across all w_{iPSS} tested (see Figure 2).

As shown in Figure 4, formulations with lightly sulfonated iPSS (f_{sulf} = 1.48 mol %) exhibit size reduction of NPs with increasing w_{iPSS} up to 5 wt %. This trend may arise from the partial miscibility between PS and lightly sulfonated iPSS, which has been observed *via* thermal analysis[51] and will be revisited later on. For intermediate f_{sulf} (5.2 mol %), progressively diminishing size reduction is observed (as previously shown in Figure 2a). Lastly, at high f_{sulf} (9.7 mol %), particle sizes are found to be larger than at lower sulfonation levels—a counterintuitive result given the greater number of charged sodium styrene sulfonate monomers present, which could provide greater electrostatic stabilization. This finding will also be revisited further below.

To gain mechanistic understanding of the formation of iPSS-stabilized NPs, we performed a series of explicit-solvent molecular dynamics simulations (see Methods Section for modeling details). We used a bead-spring model for the polymers, with iPSS chains consisting of a random distribution of styrene ("S") and sodium styrene sulfonate ("SS") monomers whose number ratio was adjusted to match f_{sulf}. We first investigated the conformation of single iPSS chains in solution, finding swollen coil-like conformations for lightly sulfonated iPSS chains ($f_{sulf} \leq$ 1.48 mol %) in THF, the starting solvent for FNP. At high sulfonation ($f_{sulf} \sim$ 10 mol %), the chain conformations fluctuated between coiled and globular states, which is reflected in the large error bars, as shown in Figure 5a. As f_{sulf} was increased even further, the iPSS chains collapsed completely. This coil-globule transition shows the balance between the solubility of the styrene units in THF

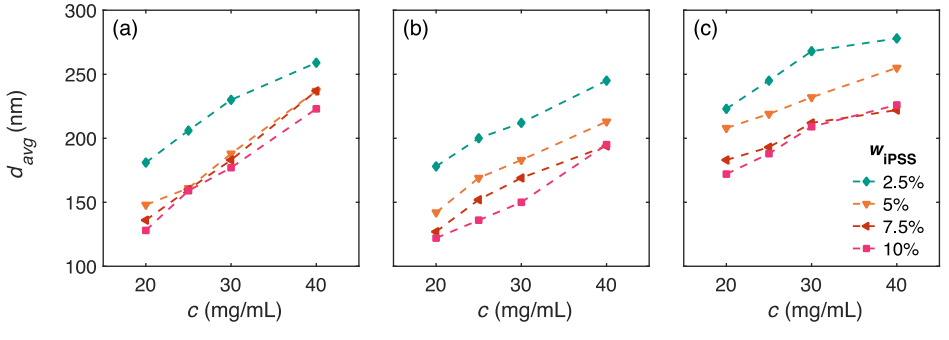

Figure 4. Effect of f_{sulf} on iPSS stabilization across a range of c and increasing w_{iPSS} for f_{sulf} = (a) 1.48, (b) 5.2, and (c) 9.7 mol %.

https://doi.org/10.1021/acs.langmuir.2c02850
Langmuir 2023, 39, 570−578

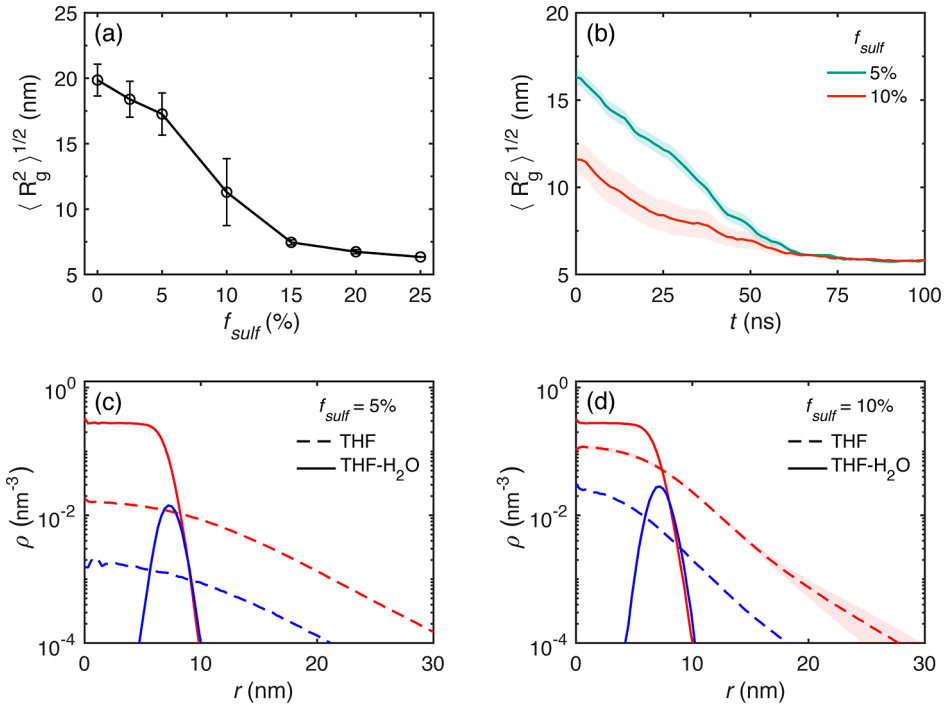

Figure 5. Simulation of single iPSS chain collapse. (a) Effect of f_{sulf} on iPSS chain conformation in solvent conditions representing THF. (b) Comparison of collapse dynamics between f_{sulf} = 5 and 10 mol % under instantaneous solvent quenching. (c,d) Radial monomer number density profiles of iPSS chains consisting of S (red) and SS (blue) monomers in initial THF (dashed curves) and final THF−H_2O mixture (solid curves).

and the insolubility of the ionic groups. This is the mirror image of the collapse of water-soluble polymer chains as the number and strength of hydrophobic residues are increased.[52,53] To test the effect of the charge distribution on the iPSS chains, we performed additional simulations using a uniform charge patterning, but did not find any appreciable effect on the average radius of gyration (R_g).

Next, to provide insights into the early stage of FNP, where fast changes in solvent quality drive the collapse of polymers prior to aggregation, we investigated the dynamics of iPSS chain conformations undergoing an instantaneous switch in solvent quality. As shown in Figure 5b, the decrease in R_g corresponds to a transition from an initial coiled (f_{sulf} = 5%) or partially collapsed (f_{sulf} = 10%) state to a fully collapsed globule. Collapse times, classified by the time when the extent of collapse reaches 99%, were found to be 76 and 78 ns for f_{sulf} = 5 and 10 mol %, respectively. This minimal variation in collapse time arises from the balance between the differences in the total range of collapse ($\Delta R_{g,5\%}^2 > \Delta R_{g,10\%}^2$) and the relative number of S monomers that drive collapse in poor solvent conditions ($n_{S,\,5\%} > n_{S,\,10\%}$). During this coil-globule transition, the R_g of the iPSS chains initially decayed as $\langle R_g^2(0)\rangle - \langle R_g^2(t)\rangle \propto t^{\alpha}$ with an exponent of $\alpha \sim 0.86 \pm 0.02$. This exponent is slightly smaller than values found in recent simulations of homopolymers under a sudden quench in solvent conditions, and we attribute the slower collapse kinetics in our simulations to the partial sulfonation of the investigated iPSS chains.[54,55]

The final globule structure of iPSS chains after collapse can provide insights into the early stages of the aggregation process inherent in FNP processing. As shown in Figure 5c,d, the SS monomer density, initially located toward the interior of chain R_g in THF, is found to completely shift to the surface of globules upon collapse in a THF−H_2O mixture for both f_{sulf} = 5 and 10 mol %. Therefore, variations in f_{sulf} manifest as changes in the surface density of SS monomers on iPSS globules. Given the enrichment of SS monomers at the surface of globules, increases in f_{sulf} may translate to a reduction in collision efficiency as higher charged iPSS globules are more electrostatically repelled by partially charged PS aggregates. This in turn can delay stabilization for high f_{sulf} iPSS chains, resulting in larger particles as seen for f_{sulf} = 9.7 mol %.

For NP formation simulations, mixtures of short PS and long iPSS chains underwent an instantaneous switch in solvent quality, resulting in their collapse and aggregation to form a single NP (Figure 6a). We systematically varied the sulfonation of the individual iPSS chains and also adjusted the number ratio of PS to iPSS chains for a fixed total mass to simulate NP formation at various w_{iPSS}. NP formation proceeded through the initial collapse of the short PS chains into compact globules, which were connected by elongated iPSS chains. These precursor aggregates then quickly contracted into a single spherical NP, often embedding small liquid droplets in the process. These trapped liquid droplets were typically surrounded by SS monomers and eventually escaped the NP *via* diffusion.

After the simulations reached equilibrium, radial density profiles of monomers were computed, relative to the NPs center of mass, to interpret the structure of the precipitated NPs. All NPs formed a core-shell structure with iPSS chains partitioning toward the NP−liquid interface, with SS monomers protruding from the NP surface. By varying formulation parameters, radial density distributions exhibited distinct trends: Variations in w_{iPSS} yielded proportional changes in both iPSS and SS distribution magnitudes while radial positioning remained invariant (Figure 6b); however, while SS monomer distributions remained at the NP surface for changes in f_{sulf}, iPSS chains collectively shifted outward from the NP

https://doi.org/10.1021/acs.langmuir.2c02850
Langmuir 2023, 39, 570−578

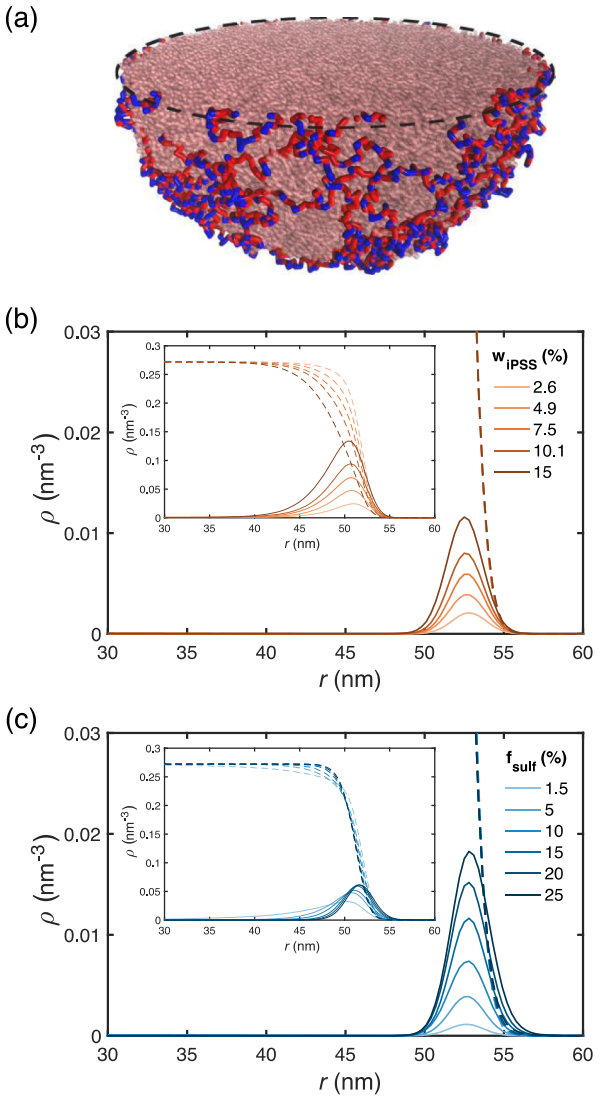

Figure 6. Simulation of NP formation from PS and iPSS chains *via* instantaneous solvent interaction switch. (a) Representative cross-sectional view of a precipitated NP with a PS core (red, translucent) and iPSS chains decorating the surface (S monomer = red; SS monomer = blue). (b,c) Radial monomer number density profiles by type (S, SS) and by polymer association (PS, iPSS) (inset) are presented for (b) increasing w_{iPSS} and fixed f_{sulf} = 5 mol % and (c) increasing f_{sulf} and fixed w_{iPSS} = 4.9%. S monomers and PS-associated monomers are represented by dashed curves; SS monomers and iPSS-associated monomers are represented by solid curves.

core as increases in the population of surface-presenting SS monomers collectively recruited more intrachain S monomers (Figure 6c).

Although iPSS chains and their constituent SS monomers were shown to partition to the NP surface due to enthalpic contributions, contributions from entropy arising from the disparity in chain lengths could affect partitioning even in the limit of $f_{sulf} \rightarrow 0$. To investigate these effects, NPs were formed from long (300 kDa) PS chains (i.e., f_{sulf} = 0%) with original 35 kDa PS chains. Converse to the surface partitioning of iPSS chains, the analogous long PS chains were found to partition toward the interior of formed NPs (Figure S1). This behavior arises due to the entropic penalty for confining long chains to the NP surface, which manifests itself as a larger interfacial tension (the difference in interfacial tension between polymers of different degree of polymerization decreases with increasing N).[56] Overall, the balance between entropically driven inward partitioning due to chain length disparity and surface partitioning resulting from enthalpically driven SS monomer exposure toward the surrounding aqueous solvent phase suggests the possibility of intermediate NP structures for low f_{sulf} formulations in which iPSS chains are partially buried. This phenomenon could further explain the negligible size reduction above w_{iPSS} = 5% for formulations containing lightly sulfonated iPSS with f_{sulf} = 1.48 mol % (Figure 4).

With insights into the formation and structure of iPSS-containing NPs, we sought to derive a design equation to predict the final particle size based on the formulation parameters. Since particle size is determined by the relative timescales of aggregation and stabilization, the time of formation (t_f) of an NP could be related to the respective concentrations of the NP core and stabilizer,[20] namely PS and iPSS for the current system. The time of formation can be approximated from the final NP diameter (d_{avg}) *via* Smoluchowski's model of DLA kinetics

$$t_f = \frac{\pi \mu \rho d_{avg}^3}{8 k_B T c_{PS,CIJ}} \tag{4}$$

where μ is the solvent viscosity (~1 mPa s), ρ is the bulk density of the core (~1050 kg/m^3), k_B is the Boltzmann constant, T is the absolute temperature (298 K), and $c_{PS,CIJ}$ is the mass concentration of PS in the CIJ mixing chamber (half of the inlet mass concentration, c_{PS}). In relating t_f to formulation parameters, a constitutive power-law ratio was proposed in accordance with prior relations defined for BCP stabilization:[20]

$$t_f = K \frac{c_{PS,CIJ}^{\alpha}}{c_{iPSS,CIJ}^{\beta}} \tag{5}$$

Fitting this relation across all formulations (c, w_{iPSS}) for each f_{sulf}, estimates for K, α, and β were obtained (Table 1). From these fits, the following observations were made. First, formulations using iPSS with f_{sulf} = 1.48 mol % cannot be precisely modeled by this relation owing to the limited size reduction for w_{iPSS} > 5%. This finding is consistent with the simulation result that high M_w iPSS chains may become buried within the PS core and their accumulation at the interface and

Table 1. Parameter Fit Estimates of Experimental Data to the Formulation Design Model (eq 2) for Each F_{sulf} Tested[a]

f_{sulf} (mol %)	K (ms mL$^{\alpha-\beta}$ mg$^{\beta-\alpha}$)	α	β	R^2
1.48	3.36 ± 2.54	1.14 ± 0.27	0.41 ± 0.14	0.797
2.45	2.76 ± 1.48	1.00 ± 0.16	0.69 ± 0.06	0.988
5.2	3.18 ± 1.15	0.95 ± 0.10	0.65 ± 0.04	0.967
9.7	20.5 ± 4.8	0.60 ± 0.08	0.46 ± 0.03	0.941

[a]Error values represent 95% confidence intervals.

https://doi.org/10.1021/acs.langmuir.2c02850
Langmuir 2023, 39, 570−578

electrostatic stabilization is not uniquely linked to the number of aggregation events during DLA. Second, the prefactor K was statistically similar for all f_{sulf} except for formulations with f_{sulf} = 9.7 mol %, indicating a significant drop in the sticking probability, assumed to be unity for DLA. Long-range electrostatic interactions between PS and iPSS aggregates and highly charged iPSS globules cause increases in repulsive forces during the aggregation process and therefore decreases in the sticking probability.[30] Third, exponents α and β were found to be ~1 and ~0.66, respectively, for formulations with intermediate f_{sulf} = 5.2 mol %.

Given the core−shell structure of iPSS-containing NPs provided by simulations, a geometric argument for stabilization by intermediate f_{sulf} iPSS, in the absence of burying (low f_{sulf}) or reduced collision efficiency (high f_{sulf}), can be proposed. The mass and therefore volume ($\sim d^3$) of the PS-rich core are proportional to c_{PS}, while the volume of the iPSS shell, in the limit of thin layer thicknesses, is dominated by surface area ($\sim d^2$). As a result, the volume of the iPSS shell is posited to scale with $\delta c_{iPSS}^{2/3}$ in which δ represents an effective thickness of the iPSS shell layer contained within the prefactor K. This scaling represents a simple volumetric ratio to describe the stabilization of core material by iPSS during FNP. To further confirm these scaling rules for intermediate f_{sulf} formulations, NPs were fabricated using an additional iPSS with an intermediate f_{sulf} = 2.45 mol %. From fits to this data set, α and β were shown to also agree with the proposed scaling (Table 1). Furthermore, although statistically similar, K is found to be larger for f_{sulf} = 5.2 mol% compared to 2.45 mol %. Since K contains and is therefore inversely proportional to δ, this result agrees with the findings from the NP formation simulations showing an outward radial shift in iPSS chain density and compression of δ with increases in f_{sulf} (Figure 6c).

To obtain a general design equation for intermediate f_{sulf} iPSS, the scaling rules (α = 1, β = 2/3) were substituted into (eq 5), and K was fit across both f_{sulf} = 2.45 and 5.2 mol % formulation sets to estimate an average K = 2.67 ± 0.09 ms mL$^{1/3}$ mg$^{-1/3}$ (see Figure S2 for a visual representation of the fit). At last, by substituting eq 5 into eq 4*via* t_f and replacing CIJ concentrations with inlet concentrations c_{PS} and c_{iPSS}, a final general design equation is obtained:

$$d_{avg} = (1.46)\left(\frac{Kk_bT}{\pi\mu\rho}\right)^{1/3}\left(\frac{c_{PS}}{c_{iPSS}^{1/3}}\right)^{2/3} \quad (6)$$

Figure 7 shows a comparison between experimental results and eq 6, demonstrating a good fit (R^2 = 0.966) and highlighting the efficacy in using eq 6 to predict average particle size from formulation parameters.

In summary, there are differences between electrostatic ionomer and steric BCP-based approaches for particle stabilization in FNP. For iPSS stabilization, t_f depends on the volumetric ratio between the PS core and iPSS shell, whereas for BCP stabilization, described by the surface adsorption of BCPs onto a hydrophobic core, t_f has been shown to relate to the ratio of respective surface areas ($t_f = K\, c_{core}^{2/3}/c_{BCP}$).[20] As a result, the NP diameter exhibits higher dependency on c_{core} for iPSS stabilization (c_{PS} in this study) compared to formulations containing BCPs (Figure S3a,b). However, equivalent particle sizes can be achieved with lower c_{iPSS} (10^{-2}−10^{-1} mg/mL) compared to those achieved by BCP stabilization ($c_{BCP} \sim 10^0$−10^1 mg/mL) (Figure S3c). In coupling these contributions with the ability to formulate with BCPs up to w_{BCP} = 100%

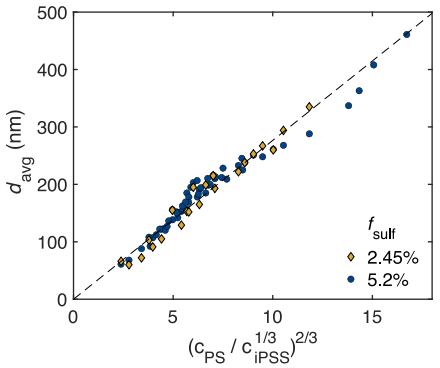

Figure 7. NP size prediction model for stabilization by intermediate sulfonated iPSS (dashed line) compared to experimental results for f_{sulf} = 2.45 and 5.2 mol %.

without trade-offs in accessible formulation space shown for iPSS stabilization (Figure 3), guidelines for the use of BCP or ionomers as stabilizers can be established: BCP stabilization enables the scalable production of sub-100 nm NPs with lower sensitivity to deviations in both c_{BCP} and c_{core} but requires w_{BCP} > 25%, suggesting its use in higher value and precise applications such as encapsulation for drug delivery. Ionomer stabilization affords NPs with larger sizes (100−250 nm) with 10-fold lower stabilizer concentration, suggesting its use for low-cost applications with higher mass throughput such as Pickering emulsifiers.

CONCLUSIONS

In this work, we demonstrated that ionomers can be used as effective stabilizers for polymeric NPs created by FNP. By exploring the formulation parameters and ionomer charge content, formulation guidelines are proposed, including the interplay between the inlet polymer concentration and the ionomer weight percent in minimizing the particle size polydispersity. By varying the charge content of ionomers, we observed optimal stabilization and size reduction *via* the use of ionomers possessing degrees of sulfonation of approximately 5 mol %. In investigating the reduction in stabilization performance with the introduction of ionomers with high charge content, molecular simulations show the fast collapse and complete outward exposure of sodium styrene sulfonate monomers for both intermediate and highly sulfonated iPSS chains, indicating a reduction in collision efficiency when using ionomers with high ionic content. In the aqueous phase, the highly charged collapsed iPSS globule is not sufficiently amphiphilic to act as an interfacial stabilizer. Additionally, simulations of NP formation reveal a core−shell structure with iPSS chains partitioning to the NP surface. This finding provides a geometric basis for the scaling exponents and prefactor obtained through fits of experimental data to a model relating formation time *via* diffusion-limited growth to component concentrations. Using this relation, a final design equation is derived, enabling the prediction of average diameters for NPs stabilized by intermediate sulfonated iPSS. As a result, FNP in conjunction with ionomer-driven stabilization has the potential to enable the scalable production of highly concentrated dispersions of charged NPs for a variety of applications. Future studies will aim to vary the chemistry of the NP core to include chemically distinct polymers or small molecules, as well as that of the ionomer stabilizers to not only investigate the generality of the formulation rules presented

https://doi.org/10.1021/acs.langmuir.2c02850
Langmuir 2023, 39, 570−578

herein but also enable the versatile fabrication of encapsulations, Pickering emulsifiers, and structured colloids.

■ ASSOCIATED CONTENT

Supporting Information

The Supporting Information is available free of charge at https://pubs.acs.org/doi/10.1021/acs.langmuir.2c02850.

Radial monomer number density profile for all-PS simulations, a visual representation of parametric fit to the constitutive relation for particle formation time, and a graphical comparison between BCP and iPSS stabilization models (PDF)

■ AUTHOR INFORMATION

Corresponding Authors

Arash Nikoubashman − *Institute of Physics, Johannes Gutenberg University Mainz, Mainz 55128, Germany;* orcid.org/0000-0003-0563-825X; Email: anikouba@uni-mainz.de

Robert K. Prud'homme − *Department of Chemical and Biological Engineering, Princeton University, Princeton, New Jersey 08544, United States;* orcid.org/0000-0003-2858-0097; Email: prudhomm@princeton.edu

Authors

Douglas M. Scott − *Department of Chemical and Biological Engineering, Princeton University, Princeton, New Jersey 08544, United States*

Richard A. Register − *Department of Chemical and Biological Engineering, Princeton University, Princeton, New Jersey 08544, United States; Princeton Institute for the Science and Technology of Materials, Princeton University, Princeton, New Jersey 08544, United States;* orcid.org/0000-0002-5223-4306

Rodney D. Priestley − *Department of Chemical and Biological Engineering, Princeton University, Princeton, New Jersey 08544, United States; Princeton Institute for the Science and Technology of Materials, Princeton University, Princeton, New Jersey 08544, United States;* orcid.org/0000-0001-6765-2933

Complete contact information is available at: https://pubs.acs.org/10.1021/acs.langmuir.2c02850

Author Contributions

‖D.M.S. and A.N. contributed equally to this work.

Notes

The authors declare no competing financial interest.

■ ACKNOWLEDGMENTS

Financial support for this work was provided by the Princeton Center for Complex Materials (PCCM), a U.S. National Science Foundation Materials Research Science and Engineering Center (grant DMR-2011750). A.N. acknowledges funding by the Deutsche Forschungsgemeinschaft (DFG, German Research Foundation) through project nos. 233630050, 274340645, 405552959, 445740352, and 470113688. The authors thank Hidemi Tomita for the synthesis and characterization of the sulfonated polystyrene ionomers. D.M.S. thanks Dr. Sarah McFann for thoughtful discussion on the geometric stabilization model.

■ REFERENCES

(1) Mitragotri, S.; Burke, P. A.; Langer, R. Overcoming the Challenges in Administering Biopharmaceuticals: Formulation and Delivery Strategies. *Nat. Rev. Drug Discovery* **2014**, *13*, 655−672.

(2) Ulbrich, K.; Holá, K.; Šubr, V.; Bakandritsos, A.; Tuček, J.; Zbořil, R. Targeted Drug Delivery with Polymers and Magnetic Nanoparticles: Covalent and Noncovalent Approaches, Release Control, and Clinical Studies. *Chem. Rev.* **2016**, *116*, 5338−5431.

(3) Lee, V. E.; Sosa, C.; Liu, R.; Prud'homme, R. K.; Priestley, R. D. Scalable Platform for Structured and Hybrid Soft Nanocolloids by Continuous Precipitation in a Confined Environment. *Langmuir* **2017**, *33*, 3444−3449.

(4) Morozova, T. I.; Nikoubashman, A. Surface Activity of Soft Polymer Colloids. *Langmuir* **2019**, *35*, 16907−16914.

(5) Morozova, T. I.; Lee, V. E.; Bizmark, N.; Datta, S. S.; Prud'homme, R. K.; Nikoubashman, A.; Priestley, R. D. In Silico Design Enables the Rapid Production of Surface-Active Colloidal Amphiphiles. *ACS Cent. Sci.* **2020**, *6*, 166−173.

(6) Leunissen, M. E.; Christova, C. G.; Hynninen, A. P.; Royall, C. P.; Campbell, A. I.; Imhof, A.; Dijkstra, M.; van Roij, R.; van Blaaderen, A. Ionic Colloidal Crystals of Oppositely Charged Particles. *Nature* **2005**, *437*, 235−240.

(7) Grundy, L. S.; Lee, V. E.; Li, N.; Sosa, C.; Mulhearn, W. D.; Liu, R.; Register, R. A.; Nikoubashman, A.; Prud'homme, R. K.; Panagiotopoulos, A. Z.; et al. Rapid Production of Internally Structured Colloids by Flash Nanoprecipitation of Block Copolymer Blends. *ACS Nano* **2018**, *12*, 4660−4668.

(8) Li, N.; Panagiotopoulos, A. Z.; Nikoubashman, A. Structured Nanoparticles from the Self-Assembly of Polymer Blends through Rapid Solvent Exchange. *Langmuir* **2017**, *33*, 6021−6028.

(9) Brugarolas, T.; Tu, F.; Lee, D. Directed Assembly of Particles Using Microfluidic Droplets and Bubbles. *Soft Matter* **2013**, *9*, 9046−9058.

(10) Liu, D.; Zhang, H.; Cito, S.; Fan, J.; Mäkilä, E.; Salonen, J.; Hirvonen, J.; Sikanen, T. M.; Weitz, D. A.; Santos, H. A. Core/Shell Nanocomposites Produced by Superfast Sequential Microfluidic Nanoprecipitation. *Nano Lett.* **2017**, *17*, 606−614.

(11) Desgouilles, S.; Vauthier, C.; Bazile, D.; Vacus, J.; Grossiord, J. L.; Veillard, M.; Couvreur, P. The Design of Nanoparticles Obtained by Solvent Evaporation: A Comprehensive Study. *Langmuir* **2003**, *19*, 9504−9510.

(12) Han, J.; Michel, A. R.; Lee, H. S.; Kalscheuer, S.; Wohl, A.; Hoye, T. R.; McCormick, A. V.; Panyam, J.; Macosko, C. W. Nanoparticles Containing High Loads of Paclitaxel-Silicate Prodrugs: Formulation, Drug Release, and Anticancer Efficacy. *Mol. Pharm.* **2015**, *12*, 4329−4335.

(13) Pagels, R. F.; Prud'homme, R. K.Inverse Flash Nano-Precipitation for Biologics Encapsulation: Nanoparticle Formation and Ionic Stabilization in Organic Solvents. *Control of Amphiphile Self-Assembling at the Molecular Level: Supra-Molecular Assemblies with Tuned Physicochemical Properties for Delivery Applications*; ACS Publication, 2017; pp 249−274.

(14) Lu, H. D.; Ristroph, K. D.; Dobrijevic, E. L. K.; Feng, J.; McManus, S. A.; Zhang, Y.; Mulhearn, W. D.; Ramachandruni, H.; Patel, A.; Prud'homme, R. K. Encapsulation of OZ439 into Nanoparticles for Supersaturated Drug Release in Oral Malaria Therapy. *ACS Infect. Dis.* **2018**, *4*, 970−979.

(15) Feng, J.; Zhang, Y.; McManus, S. A.; Qian, R.; Ristroph, K. D.; Ramachandruni, H.; Gong, K.; White, C. E.; Rawal, A.; Prud'homme, R. K. Amorphous Nanoparticles by Self-Assembly: Processing for Controlled Release of Hydrophobic Molecules. *Soft Matter* **2019**, *15*, 2400−2410.

(16) Zhang, Y.; Feng, J.; McManus, S. A.; Lu, H. D.; Ristroph, K. D.; Cho, E. J.; Dobrijevic, E. L.; Chan, H. K.; Prud'homme, R. K. Design and Solidification of Fast-Releasing Clofazimine Nanoparticles for Treatment of Cryptosporidiosis. *Mol. Pharm.* **2017**, *14*, 3480−3488.

(17) Johnson, B. K.; Prud'homme, R. K. Chemical Processing and Micromixing in Confined Impinging Jets. *AIChE J.* **2003**, *49*, 2264−2282.

(18) Lavino, A. D.; Di Pasquale, N.; Carbone, P.; Marchisio, D. L. A Novel Multiscale Model for the Simulation of Polymer Flash Nano-Precipitation. *Chem. Eng. Sci.* **2017**, *171*, 485−494.
(19) Johnson, B. K.; Prud'homme, R. K. Mechanism for Rapid Self-Assembly of Block Copolymer Nanoparticles. *Phys. Rev. Lett.* **2003**, *91*, 118302.
(20) Pagels, R. F.; Edelstein, J.; Tang, C.; Prud'homme, R. K. Controlling and Predicting Nanoparticle Formation by Block Copolymer Directed Rapid Precipitations. *Nano Lett.* **2018**, *18*, 1139−1144.
(21) Morozova, T. I.; Lee, V. E.; Panagiotopoulos, A. Z.; Prud'homme, R. K.; Priestley, R. D.; Nikoubashman, A. On the Stability of Polymeric Nanoparticles Fabricated through Rapid Solvent Mixing. *Langmuir* **2019**, *35*, 709−717.
(22) Beltran-Villegas, D. J.; Jayaraman, A. Assembly of Amphiphilic Block Copolymers and Nanoparticles in Solution: Coarse-Grained Molecular Simulation Study. *J. Chem. Eng. Data* **2018**, *63*, 2351−2367.
(23) Yan, X.; Delgado, M.; Aubry, J.; Gribelin, O.; Stocco, A.; Boisson-Da Cruz, F.; Bernard, J.; Ganachaud, F. Central Role of Bicarbonate Anions in Charging Water/Hydrophobic Interfaces. *J. Phys. Chem. Lett.* **2018**, *9*, 96−103.
(24) Nikoubashman, A.; Lee, V. E.; Sosa, C.; Prud'homme, R. K.; Priestley, R. D.; Panagiotopoulos, A. Z. Directed Assembly of Soft Colloids through Rapid Solvent Exchange. *ACS Nano* **2016**, *10*, 1425−1433.
(25) Ives, K. J.Rate Theories. *The Scientific Basis of Flocculation*; Springer: Dordrecht, 1978; pp 37−61.
(26) Tian, C.; Feng, J.; Cho, H. J.; Datta, S. S.; Prud'homme, R. K. Adsorption and Denaturation of Structured Polymeric Nanoparticles at an Interface. *Nano Lett.* **2018**, *18*, 4854−4860.
(27) Vauthier, C.; Cabane, B.; Labarre, D. How to Concentrate Nanoparticles and Avoid Aggregation? *Eur. J. Pharm. Biopharm.* **2008**, *69*, 466−475.
(28) Pansare, V. J.; Tien, D.; Thoniyot, P.; Prud'homme, R. K. Ultrafiltration of Nanoparticle Colloids. *J. Membr. Sci.* **2017**, *538*, 41−49.
(29) Binks, B. P.; Lumsdon, S. O. Pickering Emulsions Stabilized by Monodisperse Latex Particles: Effects of Particle Size. *Langmuir* **2001**, *17*, 4540−4547.
(30) Zhang, C.; Pansare, V. J.; Prud'homme, R. K.; Priestley, R. D. Flash Nanoprecipitation of Polystyrene Nanoparticles. *Soft Matter* **2012**, *8*, 86−93.
(31) Li, M.; Jiang, M.; Zhu, L.; Wu, C. Novel Surfactant-Free Stable Colloidal Nanoparticles Made of Randomly Carboxylated Polystyrene Ionomers. *Macromolecules* **1997**, *30*, 2201−2203.
(32) Li, M.; Zhang, Y.; Jiang, M.; Zhu, L.; Wu, C. Studies on Novel Surfactant-Free Polystyrene Nanoparticles Formed in Microphase Inversion. *Macromolecules* **1998**, *31*, 6841−6844.
(33) Fuentes-Ordóñez, E. G.; Salbidegoitia, J. A.; González-Marcos, M. P.; González-Velasco, J. R. Mechanism and Kinetics in Catalytic Hydrocracking of Polystyrene in Solution. *Polym. Degrad. Stab.* **2016**, *124*, 51−59.
(34) Tomita, H.; Register, R. A. Miscibility of Polystyrene-Based Ionomers with Poly(2,6-Dimethyl-1,4-Phenylene Oxide). *Macromolecules* **1993**, *26*, 2796−2801.
(35) Sauer, B. B.; Stock, R. S.; Lim, K.-H.; Ray, W. H. Polymer Latex Particle Size Measurement through High Speed Dielectric Spectroscopy. *J. Appl. Polym. Sci.* **1990**, *39*, 2419−2441.
(36) Frisken, B. J. Revisiting the Method of Cumulants for Analysis of Dynamic Light Scattering Data. *Appl. Opt.* **2001**, *40*, 4087−4091.
(37) Bishop, M.; Kalos, M. H.; Frisch, H. L. Molecular Dynamics of Polymeric Systems. *J. Chem. Phys.* **1979**, *70*, 1299−1304.
(38) Grest, G. S.; Kremer, K. Molecular Dynamics Simulation for Polymers in the Presence of a Heat Bath. *Phys. Rev. A* **1986**, *33*, 3628−3631.
(39) Jadhao, V.; Solis, F. J.; de la Cruz, M. O. Simulation of Charged Systems in Heterogeneous Dielectric Media via a True Energy Functional. *Phys. Rev. Lett.* **2012**, *109*, 223905.
(40) Lee, M. S.; Salsbury, F. R.; Brooks, C. L. Novel Generalized Born Methods. *J. Chem. Phys.* **2002**, *116*, 10606−10614.
(41) Nikoubashman, A.Chapter 7. Simulations in Polymer Colloid Formation. In *Polymer Colloids: Formation, Characterization and Applications*; Priestley, R. D., Prud'homme, R. K., Eds.; Royal Society of Chemistry, 2019; pp 240−262.
(42) Weeks, J. D.; Chandler, D.; Andersen, H. C. Role of Repulsive Forces in Determining the Equilibrium Structure of Simple Liquids. *J. Chem. Phys.* **1971**, *54*, 5237−5247.
(43) Morozova, T. I.; Nikoubashman, A. Coil-Globule Collapse of Polystyrene Chains in Tetrahydrofuran-Water Mixtures. *J. Phys. Chem. B* **2018**, *122*, 2130−2137.
(44) Polson, J. M.; Moore, N. E. Simulation Study of the Coil-Globule Transition of a Polymer in Solvent. *J. Chem. Phys.* **2005**, *122*, 024905.
(45) Anderson, J. A.; Glaser, J.; Glotzer, S. C. HOOMD-Blue: A Python Package for High-Performance Molecular Dynamics and Hard Particle Monte Carlo Simulations. *Comput. Mater. Sci.* **2020**, *173*, 109363.
(46) Li, N.; Nikoubashman, A.; Panagiotopoulos, A. Z. Multi-Scale Simulations of Polymeric Nanoparticle Aggregation during Rapid Solvent Exchange. *J. Chem. Phys.* **2018**, *149*, 084904.
(47) MacKnight, W. J.; Earnest, T. R. Structure and Properties of Ionomers. *J. Polym. Sci., Part D: Macromol. Rev.* **1981**, *16*, 41−122.
(48) Lundberg, R. D.; Makowski, H. S. Solution Behavior of Ionomers 1. Metal Sulfonate Ionomers in Mixed Solvents. *J. Polym. Sci., Part A-2* **1980**, *18*, 1821−1836.
(49) Lundberg, R. D.; Phillips, R. R. Solution behavior of metal sulfonate ionomers. II. Effects of solvents. *J. Polym. Sci., Part A-2* **1982**, *20*, 1143−1154.
(50) Xie, R.; Weiss, R. A. Molecular Dynamics Simulation of Chain Collapse of Random Ionomers in a Poor Solvent. *Comput. Theor. Polym. Sci.* **1997**, *7*, 65−74.
(51) Zhou, N. C.; Xu, C.; Burghardt, W. R.; Composto, R. J.; Winey, K. I. Phase Behavior of Polystyrene and Poly(Styrene-Ran-Styrenesulfonate) Blends. *Macromolecules* **2006**, *39*, 2373−2379.
(52) Borisov, O. V.; Zhulina, E. B. Amphiphilic Graft Copolymer in a Selective Solvent: Intramolecular Structures and Conformational Transitions. *Macromolecules* **2005**, *38*, 2506−2514.
(53) Carrillo, J. M. Y.; Dobrynin, A. V. Detailed Molecular Dynamics Simulations of a Model NaPSS in Water. *J. Phys. Chem. B* **2010**, *114*, 9391−9399.
(54) Pham, T. T.; Bajaj, M.; Prakash, J. R. Brownian Dynamics Simulation of Polymer Collapse in a Poor Solvent: Influence of Implicit Hydrodynamic Interactions. *Soft Matter* **2008**, *4*, 1196−1207.
(55) Schneider, J.; Meinel, M. K.; Dittmar, H.; Müller-Plathe, F. Different Stages of Polymer-Chain Collapse Following Solvent Quenching-Scaling Relations from Dissipative Particle Dynamics Simulations. *Macromolecules* **2020**, *53*, 8889−8900.
(56) Silmore, K. S.; Howard, M. P.; Panagiotopoulos, A. Z. Vapour−Liquid Phase Equilibrium and Surface Tension of Fully Flexible Lennard−Jones Chains. *Mol. Phys.* **2017**, *115*, 320−327.

https://doi.org/10.1021/acs.langmuir.2c02850
Langmuir 2023, 39, 570−578